PCCP

PAPER

View Article Online
View Journal | View Issue

Cite this: *Phys. Chem. Chem. Phys.*, 2014, **16**, 288

Anomalous metallic-like transport of Co–Pd ferromagnetic nanoparticles cross-linked with π-conjugated molecules having a rotational degree of freedom

Yoshikazu Ito,*[ab] Kazuyuki Takai,[a] Akira Miyazaki,[c] Vajiravelu Sivamurugan,[d] Manabu Kiguchi,[a] Yoshihiro Ogawa,[e] Naotake Nakamura,[f] Suresh Valiyaveettil,[d] Tomofumi Tada,[gh] Satoshi Watanabe[g] and Toshiaki Enoki*[a]

Received 1st September 2013,
Accepted 29th October 2013

DOI: 10.1039/c3cp53689k

www.rsc.org/pccp

We investigated the electron transport in Co–Pd ferromagnetic nanoparticles (Co 16%) cross-linked with oligo(phenyleneethynylene)diethanethiolate, which consists of three rotary phenylene moieties bridged by two acetylene groups, or icosane-1,20-dithiol, which consists of one alkane chain. Although the nanoparticles cross-linked with the alkane dithiols (the latter) have extremely high electrical resistance in electron transport, the resistance of the nanoparticles cross-linked with the conjugated molecules (the former) demonstrates a linear temperature dependence from room temperature to *ca.* 20 K; below that temperature, it has a weak temperature-dependent residual contribution with a resistance minimum around 7 K. Computational simulations suggest that the apparent metallic-like temperature dependence at high temperatures can be explained in terms of the rotational degree of freedom of the linker molecule. The rotational motion of the constituent phenylene groups, which hinders π-conjugation along the linker molecule, becomes less excited as the temperature is lowered. The successive development of a ballistic transport path through the π-conjugated linker molecule with decreasing temperature yields the metallic-like temperature dependence observed for the bridged nanoparticles. The low-temperature resistance behaviour with a minimum is a consequence of carrier scattering by the localized Co spins of Co–Pd nanoparticles randomly ordered in a ferromagnetic state that develops below the temperature of the resistance minimum.

1. Introduction

Electron transport in a random network of metallic grains has been intensively investigated as a target of electron localisation phenomena, in which Anderson localisation[1,2] occurs as a consequence of randomness in the electron transport network. In such a system, the resistance, which is described in terms of a variable-range hopping mechanism, increases exponentially in a manner unlike the behaviour of semiconductors as the temperature is lowered. Metal nanoparticles that are connected to each other behave similarly to a random network of metallic grains.[3–10] However, in contrast to metallic grains with electron localisation, it is possible to intentionally design an electronic structure of the individual constituent metallic units and obtain a well-defined unit of interconnected metal nanoparticles. In addition, the interaction between the metallic units can also be tuned using linker molecules that bridge the units.

Here, electron transport arising in the case of nanoparticles cross-linked with linker molecules is beyond the physical problem of electron localisation; instead, another important problem arises concerning electron transport in a hetero-network of metal nanoparticles and molecules. Accordingly, such systems allow us to make a variety of unconventional electronic systems based on combinations of functionalities of metal nanoparticles and linker molecules.[3–9] Motivated by this

[a] *Department of Chemistry, Graduate School of Science and Engineering, Tokyo Institute of Technology, Meguro-ku, Tokyo 152-8551, Japan. E-mail: ito@wpi-aimr.tohoku.ac.jp, tenoki@chem.titech.ac.jp*
[b] *WPI Advanced Institute for Materials Research, Tohoku University, Sendai 980-8577, Japan*
[c] *Department of Environmental Applied Chemistry, Faculty of Engineering, University of Toyama, 3190 Gofuku, Toyama-shi, Toyama 930-8555, Japan*
[d] *Department of Chemistry, National University of Singapore, 3 Science Drive 3, Singapore 117543*
[e] *Department of Chemistry, Graduate School of Science and Technology, Kumamoto University, 2-39-1, Kurokami, Kumamoto 860-8555, Japan*
[f] *Department of Applied Chemistry, College of Life Sciences, Ritsumeikan University, 1-1-1, Nojihigashi, Kusatsu, Shiga 525-8577, Japan*
[g] *Department of Materials Engineering, The University of Tokyo, 7-3-1 Hongo, Bunkyo-ku, Tokyo 113-8656, Japan*
[h] *Materials Research Center for Element Strategy, Tokyo Institute of Technology, 4259-S2-13 Nagatsuta-cho, Midori-ku, Yokohama 226-8503, Japan*

fact, we employed ferromagnetic metal nanoparticles and π-conjugated linker molecules having a rotational degree of freedom as a metallic unit and a bridging unit, respectively, to investigate how the features of the nanoparticles and linker molecules contribute to the electron transport properties of a hetero-network constructed of metal nanoparticles and π-linker molecules.

For the ferromagnetic metal nanoparticle, we employed 3 nm Co–Pd alloy nanoparticles with a Co concentration of 16 at%. According to the literature, a ferromagnetically ordered state exists in the bulk Co–Pd lattice owing to an exchange enhancement effect[11] even at an extremely low Co concentration (0.1 at%),[12] which is two orders of magnitude lower than the percolation threshold concentration $p_c \sim 2/z \sim 0.167$ (Co 16.7 at%), where $z = 12$ is the coordination number for fcc Pd.[13,14] In addition, our previous investigations of Co–Pd nanoparticles indicated that exchange enhancement produces a giant magnetic moment of 9.4 μ_B/Co for individual nanoparticles, which show superparamagnetic properties with a blocking phenomenon.[15–18] Further, for the linker molecule, we used a π-conjugated linear oligo(phenyleneethynylene) diethanethiolate (OPE diethanethiolate), which consists of three phenylene moieties bridged through acetylene groups (see Fig. 1). It is conceivable that the phenylene groups rotate with respect to the linear molecular axis at high temperatures, which reduces the conjugation. At low temperatures, the frequency of such rotation decreases, which enhances the conjugation.[19,20] Consequently, the rotation-induced conformational changes with temperature are expected to modify the electron transport through the linker molecule.[21,22]

In this work, we demonstrate that the formation of a random ferromagnetic state in the nanoparticles and the rotation-induced changes in π-conjugation of the OPE linkers govern the electron transport, on the basis of experimental investigations of the temperature dependence and magnetic field dependence of the resistance, together with magnetic measurements. Theoretical calculations of the electronic structure and electrical conductivity were also performed to validate the rotational motion of the phenylene unit in the centre of the OPE molecule at room temperature, and to understand the role of the linker molecule with a rotational degree of freedom in the electron transport with a wave-packet dynamics calculation.

2. Methods

2.1 Experimental

Pd and Co–Pd alloy nanoparticles cross-linked with OPE diethanethiolate or icosane-1,20-dithiol (C_{20} dithiol)[23,24] were prepared using a method reported earlier.[25] The nanoparticles cross-linked with C_{20} dithiol, which has no π-conjugation, were employed as a reference. A mixture of $Pd(OAc)_2$ and anhydrous $CoCl_2$ (0.5 mmol in total) and octadecanethiol (ODT, 0.10 g, 0.35 mmol) were dissolved under a N_2 atmosphere in 10 mL of freshly distilled anhydrous tetrahydrofuran (THF). To this solution, lithium triethylborohydride solution in THF (1 M, 5 mL) was rapidly added in one portion at room temperature. The resulting nanoparticles were collected by centrifugation, purified by re-dispersing the solid into THF, and then stored in THF. Network structures were formed by adding OPE diethanethiolate (0.15 mmol) or C_{20} dithiol (0.15 mmol)

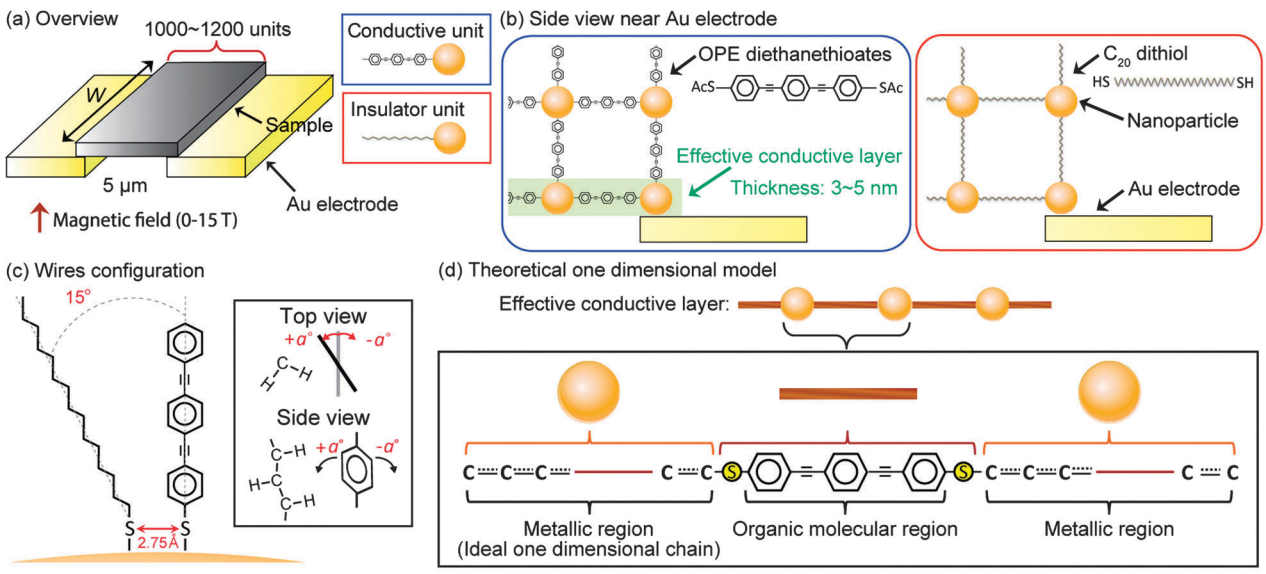

Fig. 1 Network structures with Co–Pd ferromagnetic nanoparticles and a phenylene rotary linker of OPE diethanethiolate or an alkane chain linker of C_{20} dithiol. (a) Sample having ~1000 units constructed with a nanoparticle and a linker in the space between two Au electrodes. Magnetic fields were applied perpendicular to the film sample. (b) Schematic of the structural organization near the Au electrode and rotary linker (left) and alkane chain linker (right). The network is shown as a squared lattice for simplicity, although the actual sample is a random network. The green shaded area shows an effective conductive layer (3–5 nm) in the nanoparticle network. (c) Computational model of configuration of an OPE molecule and alkane thiol wires on a nanoparticle for rotational barrier calculations. Top and side views parallel to the OPE wire axis are also shown, together with the definition of the phenylene rotation angle *a* with alkane chains. The grey and black lines correspond to the bottom and central benzene fragments, respectively, projected along the molecular axis. (d) Theoretical one-dimensional model combined with the metallic region and the organic molecular region.

to the suspension of the Co–Pd alloy nanoparticles in the same batch and stirring the mixture for 24 h at room temperature. The resulting solution was centrifuged, and the solid residue collected was washed with hexane, dried, and used for further studies.

The Co : Pd atomic ratios of the nanoparticles were determined using inductively coupled plasma-optical emission spectroscopy (PerkinElmer Optima 5300 DV spectrometer), and the amount of the organic capping agent on the surface of the nanoparticles before and after cross-linkage was obtained by elemental analysis. Their morphology was characterized using transmission electron microscopy (TEM) and electron diffraction with a JEOL TEM-2010F electron microscope equipped with a diffractometer operating at an acceleration voltage of 200 kV. Samples were prepared by placing a hexane suspension of nanoparticles on carbon-coated Cu grids and allowing it to dry at room temperature. The magnetic susceptibility and magnetisation were measured with a Quantum Design MPMS-7 SQUID magnetometer up to a field of 7 T at temperatures of 2–300 K. The temperature dependence of the magnetisation was measured under 0.01 T from 2 K to room temperature for a heating run after zero-field cooling (ZFC) and field cooling (FC) under 0.01 T. The electrical resistance was measured with a quasi-four-terminal method at temperatures of 2.6–300 K under a magnetic field of up to $\pm$15 T using an Oxford TESLATRON instrument. In the transport measurement, the agglomerates in the hexane solution were dropped and dried on Au electrodes (Au Interdigitated Array Electrode, BAS Inc.), which had an electrode width, an inter-electrode interval, and a number of feet (pairs) of 10 μm, 5 μm, and 65, respectively. The TEM images indicated that the number of neighbouring nanoparticles surrounding a nanoparticle was *ca.* 6–8, as will be discussed later. From the size of the electrodes together with the number of neighbouring nanoparticles, we can estimate that the inter-electrode interval is spanned by *ca.* 1000–1200 nanoparticle–OPE diethanethiolate–C_{20} dithiol hybrid units if we simplify the nanoparticle/linker molecule network to form a simple cubic lattice (with coordination number 6) consisting of nanoparticle–OPE diethanethiolate–C_{20} dithiol units (see Fig. 1). The applied voltage was kept below 0.1 V to maintain a linear *I–V* response. The temperature dependence and magnetic field dependence of the resistance were measured under an applied voltage of 7.5×10^{-4} V.

2.2 Theoretical calculations

The electronic state of an OPE diethanethiolate molecule, in which three constituent phenyl groups rotate with respect to its molecular axis under the influence of surrounding alkane thiolate linear molecules (number of carbons: 15), was calculated using the Gaussian 09 code.[26] We made computational models in which we set the distance between the sulphur atom of the OPE linear molecule and the sulphur atom of the neighbouring alkane molecule to 0.275 nm, corresponding to the closest distance between the *fcc* adsorption sites on the Pd(111) surface. Further, the tilt angle of the wire axis of the alkane thiolate was fixed at 15° with respect to the axis of the OPE molecule, which was derived from the following conditions: (i) the S–S nearest distance is 0.275 nm, (ii) the nanoparticles are a few nanometres in diameter, and (iii) the organic molecules are extended in straight lines in all directions from the centre of the nanoparticle, as shown in Fig. 1(c). In addition to the above restrictions, the rotation angle of the central phenylene units in the OPE molecule was also limited to the range from −90 to 90° in the structural optimisations to calculate the potential energy surface of the phenylene rotation. The rotation angle was defined as the mutual angle between the molecular planes of adjacent phenyl groups [see Fig. 1(c)]. The computations were performed as follows: (i) the B3LYP hybrid density functional[27,28] method with the 6-31G(d,p) basis set was adopted in the structural optimisations with the above restrictions, and (ii) MP2[29] electron correlation calculations with the 6-31G(d,p) basis set were performed using the optimized structures. The two steps were executed for each configuration of the OPE molecule. Those calculations were made to determine the possibility of benzene rotation even near the alkane wire; the rotation was found to be plausible at room temperature, as will be discussed in the Results section.

For the second class of simulations, the conductivity of the nanoparticles cross-linked with OPE diethanethiolate was calculated using molecular dynamics (MD) in the GGA-PBE/SZP level[30] of the density functional theory (DFT) in SIESTA[31] and wave-packet scattering simulations.[32] In the scattering simulations, the nanoparticles cross-linked with the OPE molecules were modelled by an effective one-dimensional tight-binding chain consisting of metallic and organic molecular regions, as shown in Fig. 1(d). In addition, a bare OPE wire was adopted in the first-principles MD simulations to simplify the computational model. Because the possibility of benzene rotation in OPE under realistic conditions was confirmed in the electron correlation calculations (rotational angles $\pm$15° are realistic for OPE without alkane chains as shown in Table 1), the assumption for the simple modelling can be considered reasonable.

The simulation involved five steps: (i) *ab initio* MD calculations for an OPE molecule with two terminating sulphurs for 30 ps at 10, 15, 25, 50, and 70 K; (ii) determining the time dependence of the Hamiltonian matrices[33] for an effective tight-binding chain with 1000 units connected in the linear mode using the trajectories in (i) for each temperature;

Table 1 Calculated total energy E_i with an alkane chain and the normalized Boltzmann factors at room temperature for the rotation of the central benzene fragment. Calculated total energy E without an alkane chain is listed for comparison

Rotation angle (°)	E_i (meV)	Boltzmann factor	E (meV)
−90	79.78	0.01	—
−75	57.16	0.02	—
−60	33.38	0.05	—
−45	16.69	0.10	—
−30	17.13	0.10	9.43
−15	15.30	0.10	1.31
0	17.60	0.09	0.00
15	8.26	0.14	1.31
30	0.00	0.19	9.43
45	9.34	0.13	—
60	29.61	0.06	—
75	59.51	0.02	—

(iii) quantum wave-packet scattering simulations with the time dependence of the Schrödinger equation based on the time dependence of the Hamiltonian matrices in (ii); (iv) calculations of the diffusion coefficients $D = \lim\{<r^2(t)> - <r(t)>^2\}/2t$ $(t \rightarrow +\infty)$[34] from the scattered (*i.e.* propagated) wave packets, and the charge mobility obtained using the Einstein relationship ($\mu = De/k_BT$) at each temperature, where r, t, k_B, and T are the position vector, simulation time, Boltzmann constant, and temperature, respectively. Step (v), calculation of the resistance of the nanoparticles cross-linked with OPE diethanethiolate, was performed using the equation

$$R(\Omega) = \frac{1}{nFQ\mu_{cal}}\frac{L}{S}, \quad (1)$$

where n is the density of conduction electrons, F is the volume fraction of Pd nanoparticles in the sample, Q is an elementary charge, and S and L are the area of the sample and the distance between the electrodes with respect to the experimental configuration of the sample, respectively [see Fig. 1(a) and (b)]. Here we assumed that only the first layer with a cubic lattice on the electrodes participates in electron transport, as the current is distributed mostly in the first layer, as shown in Fig. 1(b).

3. Results

The Co concentration of Co–Pd alloy nanoparticles was estimated as 16 at%, whereas the elemental analysis indicates a weight per cent of ODT of 69.2% before the cross-linkage. The number of ODT molecules was calculated as 300–400 on each nanoparticle surface. After the cross-linkage, the weight per cent of the organic component (ODT + OPE diethanethiolate) increased by 4%. This increase revealed that 30–40 OPE diethanethiolate molecules existed on the surface of each nanoparticle, and *ca.* 10% of the ODT molecules were replaced by OPE diethanethiolates. Fig. 2 shows TEM images of the Co–Pd alloy nanoparticles before and after cross-linking with OPE diethanethiolate. Before cross-linking, well-dispersed nanoparticles were observed as a homogeneous sphere [inset of Fig. 2(a)]. The average diameter is 2.9 ± 0.3 nm for the pure Pd nanoparticles (Co 0 at%) and

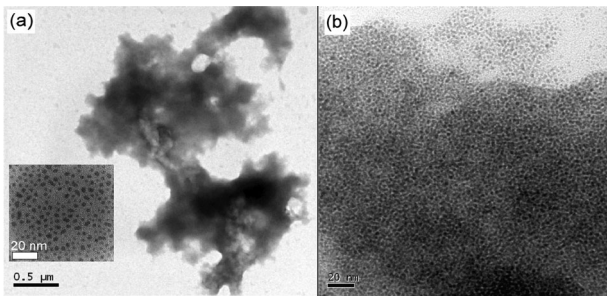

Fig. 2 TEM images of (a) 3 nm Co–Pd alloy nanoparticles cross-linked with OPE diethanethiolate and (b) the same nanoparticles with higher magnification. Inset in (a) is a TEM image of well-dispersed Co–Pd alloy nanoparticles before cross-linkage. Scale bars in (a) and (b) are 0.5 μm and 20 nm, respectively.

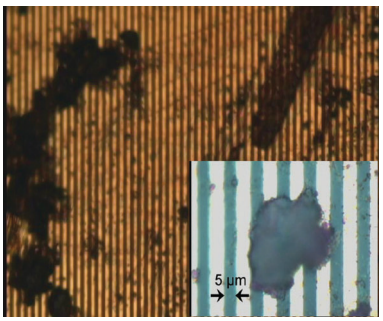

Fig. 3 Optical images of Co–Pd alloy nanoparticles on a Au electrode on a patterned substrate after cross-linking with the OPE dithiolate. Inset shows a magnified image of the agglomerates. Black stains are samples dropped and dried on the substrate. Bright stripes are Au electrodes (10 μm); dark stripes are glass substrate whose width is 5 μm.

3.0 ± 0.3 nm for the Co–Pd nanoparticles with Co 16 at%. The structure of the nanoparticles was characterized as an *fcc* structure from the electron diffractions.[15,16] Co–Pd alloy nanoparticles (3 nm, Co 16 at%) cross-linked with C_{20} dithiol were similarly characterized in a previous work.[25] The average number of molecules (ODT + C_{20} dithiol) on the surface of each nanoparticle was 300–400, 25–35 of which were assigned to C_{20} dithiol molecules.

After cross-linking, large agglomerates were observed, as shown in Fig. 2(a). The well-packed nanoparticles are visible in the agglomerate in Fig. 2(b). Moreover, the number of neighbouring nanoparticles surrounding a nanoparticle was roughly estimated as 6–8 from several enlarged TEM images for nanoparticles cross-linked with both OPE diethanethiolate and C_{20} dithiol. Fig. 3 shows optical microscope images of the sample dropped on a glass substrate with Au electrodes.

The magnetic moment was estimated as 340 μ_B/particle for the Co–Pd (Co 16 at%) nanoparticles without cross-linking from the saturation magnetisation at 2 K, whereas that of the nonmagnetic Pd nanoparticles was 2.3 μ_B/particle.[15,16] Fig. 4 shows the magnetisation (M) of the Co–Pd particles cross-linked with OPE diethanethiolate (abbreviated as Co–Pd/OPE)

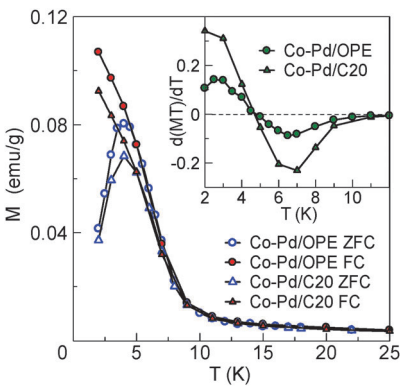

Fig. 4 Temperature dependence of magnetisation M. Circles and triangles represent Co–Pd/OPE and Co–Pd/C_{20} network samples, respectively. Open and closed symbols denote ZFC and FC at 0.01 T, respectively. Inset shows d(MT)/dT under ZFC.

and with C_{20} dithiol (abbreviated as Co–Pd/C_{20}) under ZFC and FC, together with the temperature dependence of the derivative d(MT)/dT. Both derivatives decrease as the temperature is lowered below *ca.* 10 K, and then it increases after a minimum at *ca.* 7 K. The upward change in d(MT)/dT below 7 K suggests the onset of ferromagnetic ordering. The difference in the behaviour between the zero-field cooled and field cooled conditions and the appearance of a peak in the magnetisation at 4–5 K in the zero field process indicate a blocking phenomenon occurring at 4–5 K. The occurrence of a blocking phenomenon is important evidence that the nanoparticles are well separated from each other, proving that they are not fused to each other.[25]

The resistance of the Co–Pd/C_{20} network sample without π-conjugation was ∼0.5 MΩ at room temperature, which is three to four orders of magnitude larger than that of the Co–Pd/OPE network sample. This suggests that the π-conjugation in the linker molecules plays an essential role in electron transport. Fig. 5(a) shows the typical temperature dependence of the resistance for the Co–Pd/C_{20} and Co–Pd/OPE network samples, where the resistance value is normalized with respect to the value at room temperature. In the Co–Pd/OPE network sample, the absolute value of the resistance changes in a wide range of 10–300 Ω at room temperature depending on the samples, as the shape and amount of the network sample dropped on the electrodes varied widely by chance. This behaviour was reproduced, and we found that both Pd and Co–Pd nanoparticles show a similar tendency.

Note, however, that the temperature dependence of the normalized resistance value has no sample dependence. The resistance measured from 2.6 to 300 K with $V = 7.5 \times 10^{-4}$ V shows no difference between the cooling and heating processes in the Co–Pd/OPE network sample. The resistance decreases linearly as the temperature is lowered to *ca.* 20 K, and below that temperature it becomes less temperature dependent, with a residual resistivity of R(0 K)/R(300 K) = 0.31. The linear temperature dependence of the resistance suggests apparently metallic transport in the Co–Pd metallic nanoparticles bridged by OPE dithiolate linker molecules. Fig. 5(b) shows the I–V characteristic of the Co–Pd/OPE network samples measured at 4.2 K, 126 K, and 300 K. It confirms the Ohmic behaviour between −0.1 and +0.1 V at temperatures of 4.2–300 K. Taking into account the number of units present between the electrodes (see Fig. 1), the effective applied voltage to each unit is simply calculated as *ca.* 0.1 mV. At this small voltage magnitude, the I–V curve of OPE dithiol in single molecular conductivity reportedly exhibits linearity.[35] This is in good agreement with the behaviour observed in Fig. 5(b).

The resistance behaviour in the Pd/OPE network samples is almost the same as that in the Co–Pd/OPE network samples except at low temperatures. Fig. 5(c) and (d) show close-ups of the temperature dependence of the resistance at low temperatures for the Co–Pd/OPE and Pd/OPE network samples, respectively, without applied magnetic fields. A specific difference between the Co–Pd/OPE and Pd/OPE network samples is observed in the resistance behaviour. The Co–Pd/OPE network sample has a resistance minimum at around 7–8 K, whereas the

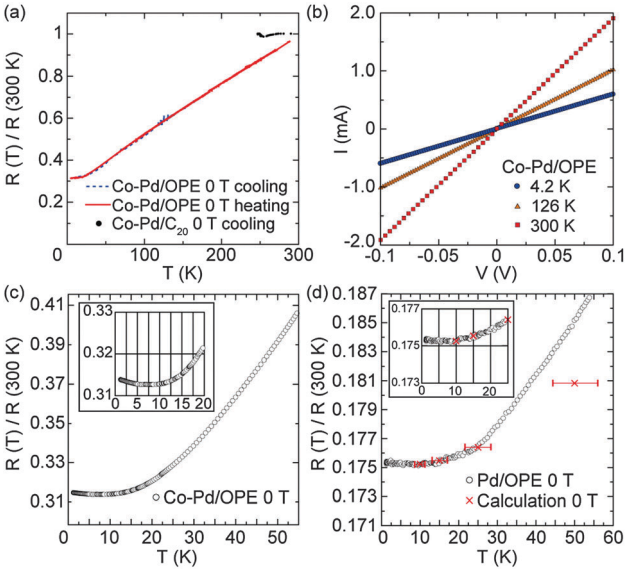

Fig. 5 Electron transport properties of Co–Pd/OPE (Co 16 at%), Co–Pd/C_{20} (Co 16 at%), and Pd/OPE network samples. (a) Temperature dependence of resistance. Solid and dotted lines represent results of measurement under cooling and heating processes, respectively. Circles represent Co–Pd/C_{20}. (b) I–V curves of Co–Pd/OPE network sample. Circles, triangles, and squares represent resistance at 4.2 K, 126 K, and 300 K, respectively. (c) and (d) close-ups of Co–Pd/OPE and Pd/OPE network samples, respectively, at low temperatures. Theoretical result (cross symbols) from wave-packet dynamics combined with MD calculation is also shown in (d). Error bars for calculated resistance correspond to temperature fluctuations in MD calculations. Calculated resistance is fitted with the experimental one by adding residual resistance R(0 K)/R(300 K) of 0.1758 to raw calculated values. The inset shows a magnified view of the lower-temperature region.

Pd/OPE network shows only a plateau. In addition, the residual resistance at $T = 0$ K is larger in the former than in the latter; R(0 K)/R(300 K) = 0.31 and 0.18 for the Co–Pd/OPE and Pd/OPE network samples, respectively.

The magnetic field dependence of the resistance appears for the Co–Pd/OPE network sample in the low-temperature region below *ca.* 20 K, in contrast to the negligible magnetoresistance in the Pd/OPE network sample, as shown in Fig. 6. The change between 0 T and 15 T in the Co–Pd/OPE network sample shows an increase of 1.5% at 2.6 K. The magnitude of the magnetoresistance

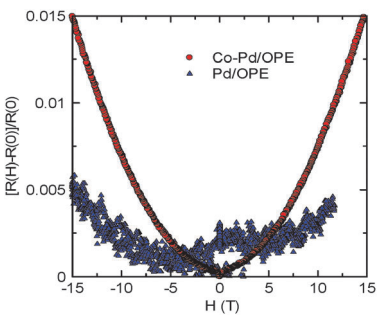

Fig. 6 Magnetic field dependence of resistance of Co–Pd/OPE (circles) and Pd/OPE (triangles) network samples at 2.6 K.

is smaller than that in the bulk analogue, which is reportedly +5%/−1%.[36,37] In contrast, the resistance increase between 0 T and 15 T in Pd/OPE is only ~0.5% at 2.6 K.

4. Discussion

First, let us discuss the metallic-like behaviour of electron transport in the high-temperature regime. A random network of metallic domains generally shows simple variable-range hopping or Coulomb-gap-type variable-range hopping,[3–9] in which the resistance increases with decreasing temperature. This disagrees entirely with our observation of metallic-like resistance behaviour. Consequently, the origin of the metallic-like electron transport needs to be discussed using another mechanism. Here, the heterostructure of the nanoparticle and linker molecule may be responsible for the metallic-like behaviour. However, there have been no reports of metallic-like behaviour in nanoparticles cross-linked by organic molecules, to the best of our knowledge.[3–10] A clue to finding a possible mechanism is offered by a recent report,[38] which demonstrates that the resistance of 10 nm Au nanoparticles cross-linked with conjugated molecules is described not by the Coulomb blockade, but in terms of a series of resistances of nanoparticle-linker molecule units. In our case, elemental analysis, TEM, and optical image observations indicate that the nanoparticles are cross-linked by OPE diethanethiolate in the aggregates placed on the electrodes, where 30–40 linker molecules of OPE diethanethiolate per nanoparticle participate in the cross-linkage. Thus, our cross-linkage system is thought to be similar to the reported mechanism in terms of the resistance series; further, such a cross-linked system can be modelled as a random hetero-network of metal nanoparticles and linker molecules, as shown in Fig. 1.

Here the metal nanoparticles cannot be responsible for the observed metallic-like transport because there is no direct contact between the nanoparticles owing to the presence of linker molecules bridging them. This conjecture is experimentally supported by the following findings: (i) the difference in the resistance between the Co–Pd/C_{20} and Co–Pd/OPE samples and (ii) the presence of a blocking phenomenon in the magnetic behaviour. The resistance of the Co–Pd/C_{20} network sample with no π-conjugation in the linker molecule is extremely high, in the range of 0.5 MΩ, whereas that of the Co–Pd/OPE sample with π-conjugation is 10–300 Ω. The extremely high resistance of the former allows us to exclude the fusion of metal nanoparticles, which might result in metallic conduction, and the low resistance in the latter suggests that linker molecules in the Co–Pd/OPE network are responsible for the high electrical conduction.

We can discuss the absence of fusion in another way according to the observed magnetic properties. If the metallic-like resistance in the Co–Pd/OPE network is a consequence of metallic conduction in fused metal nanoparticles, the metallic conduction network should be continuously extended with no region in which fusion is absent between the two electrodes with an inter-electrode distance of 5 μm. According to percolation theory,[13,14] an extended network can be possible if each nanoparticle is connected by metallic conduction paths with at least two of the neighbouring nanoparticles. In the randomly packed nanoparticles, the number of neighbouring nanoparticles is roughly estimated as $z \sim 6$–8 (almost close packed). Accordingly, the percolation threshold above which the metallic conduction network is extended is estimated as $2/z = 2/(6–8) \sim 0.25$–0.33. This means that 25–33% of the nanoparticles should be fused to make the metallic electrical conduction paths. However, this contradicts the presence of a blocking phenomenon in the present experiment. A large concentration of fused superparamagnetic nanoparticles cannot show any blocking phenomenon, as discussed previously.[25]

Therefore, we conclude that the linker molecules are the origin of the metallic-like transport. In the linear linker molecule consisting of alternating phenyl groups and acetylene groups, the rotational degrees of freedom of the phenyl groups significantly influence the electron transport across the π-conjugated system.[39,40] Namely, the rotational motion excited at high temperatures, which destroys the conjugated π-electronic system, disturbs the electron transport in the linker molecule. In contrast, the π-conjugated electronic state is formed in the entire linker molecule at low temperatures, at which the rotational motion is less excited, producing a coherent electron transport path in the linker molecule. This can lead to the observed metallic-like temperature dependence of the resistance.

To verify the validity of the above conduction mechanism using MD theoretical approaches, let us simplify the network structure as a hybrid unit consisting of a nanoparticle (3 nm) and an OPE diethanethiolate (sulphur-to-sulphur distance: *ca.* 1.9 nm). When the units are assumed to be linearly aligned inside the aggregates on the substrate, as shown in Fig. 1, *ca.* 1000 units exist between the electrodes (gap: 5 μm). Moreover, owing to the rigid structure of the unit, it is conceivable that the network structure is not altered by the application of a magnetic field. This is justified by our previous work[25] and also by the absence of hysteresis in the resistance in the field sweeping process between −15 T and 15 T.

Here, we assume that the temperature dependence of the resistance at high temperatures originates from the rotating benzene rings in the OPE linker bridging the nanoparticles. Namely, the resistance of the network system is negligible when the π-conjugated system is intact along the linker molecule, in addition to the negligible contribution of the tunnelling barrier between the edge of the metal nanoparticle and the sulphur atoms of the OPE diethanethiolate.[41] In other words, only the rotation of benzene rings, which destroys the π-conjugated system, is responsible for the observed temperature-dependent behaviour of the resistance. In fact, the dihedral angles between neighbouring benzene rings can be larger with increasing temperature, significantly reducing the electron transport. Here our previous work[42] and reports by Allara *et al.*[43,44] provide evidence supporting the present model, in which the rotational motion plays an essential role. In the former, the acetylene and phenylene moiety covered by α-cyclodextrin was significantly rotated at room temperature, whereas the latter reported that the thermal-activation-type conductance of an OPE

molecule with a NO_2 functional group in the centre benzene ring surrounded by self-assembled monolayers demonstrated a minimum resistance at 30 K, and it concluded that a rotation-induced transition from incoherent to coherent conduction occurred.

Note that the intermolecular interaction of the OPE linker molecule with surrounding molecules affects the activated rotational motion of the phenylene units. To elucidate this effect in the present system shown in Fig. 1(c), the total energy calculation of the OPE linker molecule, in which the rotational motions of the constituent phenyl groups are affected by the surrounding alkane thiolate molecules, yields important information. The total energies calculated with MP2/6-31G(d,p) are shown in Fig. 7(a).

From the calculation results, the configuration with a rotation angle of 30° is the most stable, as shown in Fig. 7(b). From the calculated potential energy surface, the probability of each configuration at room temperature is obtained by using the Boltzmann factor, as listed in Table 1. The calculated Boltzmann factors indicate that the configurations of the rotated central benzene between −45° and 45° can be expected to appear during the conductance measurements. In particular, the three configurations with rotation angles of 15°, 30°, and 45° are the main OPE structures. To confirm the possibility of orbital localisation/delocalisation by the benzene rotation, the highest occupied molecular orbitals (HOMOs) in the three main configurations are depicted in Fig. 7(c–e). The HOMOs of the benzene rotated by 15° and 30° are delocalized well in the OPE wire, but the HOMO with 45° rotation is localized, leading to a broken path for electron transport. We also confirmed that the lowest unoccupied molecular orbitals (LUMOs) of the three main configurations show similar localisation or delocalisation of the orbitals. Therefore, the theoretical calculation, together with the experimental observation, allows us to conclude that the rotation of the phenylene units can be thermally activated,

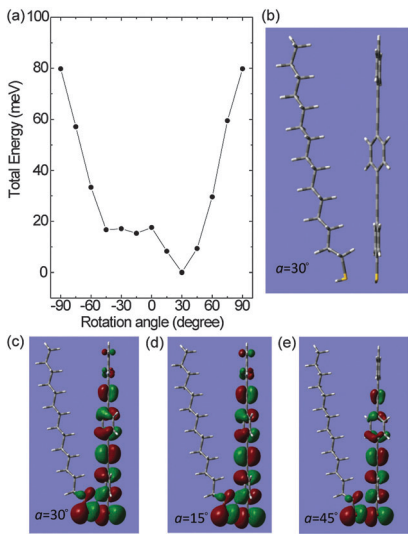

Fig. 7 (a) Calculated MP2 energies of rotating-phenylene configurations. (b) Optimized structure for 30° rotation of central benzene fragment. (c–e) HOMOs of the 30°-, 15°-, and 45°-rotated configurations. See Fig. 1(c) for the definition of angle *a*.

Table 2 Mobility and resistance calculated with the MD method and observed resistance of Pd network samples at *T* K. Fitting the calculated results with the experimental ones gives a residual resistivity of *R*(0 K)/*R*(300 K) of 0.1758 [see also Fig. 5(d)]

	Temperature *T* (K)				
	10	15	25	50	70
Mobility ($m^2\ V^{-1}\ s^{-1}$)	20.96	13.05	5.34	1.39	0.67
Calculation of $R(T\ K)/R(300\ K)$ (10^{-4})	3.70	5.93	14.4	55.7	115.6
Experimental $R(T\ K)/R(300\ K)$ (10^{-4})	3.70	5.93	15.1	95.6	187.0
Difference in the resistance (%)	0	0	4.9	42	38

and in turn the rotation results in orbital localisation, which reduces the electron transport probability. Moreover, the benzene rotational motion is less activated owing to the presence of an alkane chain near the OPE molecule, as shown by the comparison in Table 1.

Now let us calculate the conductivity of the Co–Pd/OPE network sample with rotating phenyl groups. In the MD calculation, the metal nanoparticles are simplified as a one-dimensional metallic π-conjugated carbon chain, as shown in Fig. 1(d). This simplification makes the conductivity calculation feasible using the wave-packet scattering method and MD calculations in which hybrid units form a one-dimensional chain, as shown in Fig. 1(d). In the wave-packet simulation, we used a localized wave packet with the Fermi velocity of a one-dimensional metallic chain and a half-width of 0.015τ as the initial wave packet, where τ is the transfer integral between neighbouring carbon atoms in the metallic regions in Fig. 1(d). Wave-packet simulations for 5 ps are sufficient to obtain steady-state wave-packet diffusion (*i.e.* a constant diffusion coefficient *D*).[45] Using the diffusion coefficients, we can calculate the mobility μ_{cal} and the resistance of the network samples from eqn (1). Here we adopted typical values of 10^{-22} cm^{-3} for *n*, 5 μm for *L*, 5 nm × 30 μm for *S*, and 1/10 for F.[46] The calculated resistance is shown in Fig. 5(d) and summarized in Table 2, which shows a negligibly small dependence on temperature up to 15 K and an abrupt increase from 15 K, which is similar to the experimentally observed changes in the resistance. Interestingly, the calculated value of *R*(0 K)/*R*(300 K) and the temperature dependence of the resistance are in good quantitative agreement with those observed below 25 K, as confirmed in Table 2 and Fig. 5(d). Accordingly, we can conclude that the metallic-like temperature-dependent term can be explained by thermally activated resistance caused by the changes in electron transport due to rotation of the benzene rings in the OPE diethanethiolate.

Next, we discuss the contribution of metal nanoparticles to the resistance. The large residual resistance (*R*(0 K)/*R*(300 K) = 0.31 and 0.18) for the Co–Pd/OPE and Pd/OPE network samples, respectively, cannot depend solely on the contribution of the linker molecules, as discussed above. Instead, the metal nanoparticles and the contact resistance between the nanoparticles and the linker molecules are expected to contribute significantly. Indeed, the differences in behaviour between the Co–Pd and Pd nanoparticles cross-linked with the same OPE linker with regard to the residual resistance confirms the contribution from the nanoparticles used. Namely, the presence of a resistance minimum

at 7 K, the large residual resistance, and the large magnetoresistance in the Co–Pd network sample suggest a contribution from the ferromagnetic state of the individual Co–Pd nanoparticles, considering that the Pd network sample does not show such behaviour. The sharp increase in the value of d(MT)/dT below 7 K supports the onset of ferromagnetic ordering, as shown in Fig. 4. At the same temperature, a resistance minimum was also observed for the Co–Pd/OPE network sample [Fig. 5(c)]. Accordingly, the resistance minimum is considered to be related to the effect of ferromagnetic ordering in the individual ferromagnetic Co–Pd nanoparticles below that temperature. Note that the Co concentration (16%) in the Co–Pd nanoparticles is just below the percolation threshold concentration (16.7%). This means that the co-existence of direct Co–Co exchange interactions and the interatomic-distance-dependent RKKY interaction in the random network of Co atoms produces a disordered ferromagnetic state in the individual nanoparticles. This ferromagnetic state has a spontaneous magnetization (ferromagnetically aligned) but the directions of magnetic moments of Co ions have random deviations. Consequently, the randomness in the spin arrangement contributes to the electron scattering in each nanoparticle in the conductive pathways, resulting in the increase in the resistance below 7 K in the conductive hetero-network.

5. Conclusions

We demonstrated anomalous metallic-like transport behaviour in a hetero-network constructed of Co–Pd ferromagnetic nanoparticles bridged by OPE diethanethiolates having rotationally flexible phenylene units. The conductivity shows metallic-like behaviour at high temperatures and a large residual resistivity with a resistance minimum at *ca.* 7 K at low temperatures. The metallic-like conductivity can be understood in terms of thermally activated rotation of the phenylene units of the OPE diethanethiolates, which leads to a decrease in the electron conduction in the linker molecule between the metal nanoparticles at high temperatures as a consequence of degradation of the π-conjugated electronic system. The resistance minimum in the residual resistance is concluded to be due to the development of a random ferromagnetic state in the Co–Pd ferromagnetic nanoparticles.

Author contributions

Y.I. prepared and characterized the nanoparticle/organic molecule hybrid. Y.I., K.T, and A.M. performed the measurements. T.T. and S.W. performed the computational simulation. V.S. and S.V. synthesized the OPE molecule. Y.O. and N.N. synthesized the C_{20} dithiol. Y.I., K.T., M.K., T.T., and T.E. wrote the paper. T.E. planned the project. All authors discussed the results and contributed to the manuscript.

Acknowledgements

Financial support for part of this work was provided by MEXT/JSPS KAKENHI Grant Numbers 19051006, 20001006, and 22760534 from the Ministry of Education, Culture, Sports, Science and Technology (MEXT), Japan, and by the Agency for Science, Technology and Research (ASTAR), Singapore. Y.I. was supported by a JSPS Fellowship. T.T. acknowledges the use of computational resources at the Tokodai Institute of Element Strategy.

Notes and references

1 P. W. Anderson, *Phys. Rev.*, 1958, **109**, 1492–1505.
2 P. A. Cox, *The Electronic Structure and Chemistry of Solids*, Oxford University Press, Oxford, 1987.
3 J. M. Wessels, H.-G. Nothofer, W. E. Ford, F. V. Wrochem, F. Scholz, T. Vossmeyer, A. Schroedter, H. Weller and A. Yasuda, *J. Am. Chem. Soc.*, 2004, **126**, 3349–3356.
4 C. Chu, J. A. Ayres, D. M. Stefanescu, B. R. Walker, C. B. Gorman and G. N. Parsons, *J. Phys. Chem. C*, 2007, **111**, 8080–8085.
5 P. Banerjee, D. Conklin, S. Nanayakkara, T.-H. Park, M. J. Therien and D. A. Bonnell, *ACS Nano*, 2010, **4**, 1019–1025.
6 T. Sugawara, M. Minamoto, M. M. Matsushita, P. Nickels and S. Komiyama, *Phys. Rev. B: Condens. Matter Mater. Phys.*, 2008, **77**, 235316.
7 S. Taniguchi, M. Minamoto, M. M. Matsushita, T. Sugawara, Y. Kawada and D. J. Bethell, *Mater. Chem.*, 2006, **16**, 3459–3465.
8 R. P. Tan, J. Carrey, C. Desvaux, L.-M. Lacroix, P. Renaud, B. Chaudret and M. Respaud, *Phys. Rev. B: Condens. Matter Mater. Phys.*, 2009, **79**, 174428.
9 R. P. Tan, J. Carrey, C. Desvaux, J. Grisolia, P. Renaud, B. Chaudret and M. Respaud, *Phys. Rev. Lett.*, 2007, **99**, 176805.
10 A. Zabet-Khosousi, P.-E. Trudeau, Y. Suganuma, A.-A. Dhirani and B. Statt, *Phys. Rev. Lett.*, 2006, **96**, 156403.
11 T. Moriya, *Prog. Theor. Phys.*, 1965, **34**, 329.
12 R. M. Bozorth, P. A. Wolff, D. D. Davis, V. B. Compton and J. H. Wernick, *Phys. Rev.*, 1961, **122**, 1157.
13 D. Stauffer and A. Aharony, *Introduction To Percolation Theory*, Taylor & Francis, 1994.
14 S. Kirkpatrick, *Rev. Mod. Phys.*, 1973, **45**, 574–588.
15 A. Miyazaki, Y. Ito and T. Enoki, *Eur. J. Inorg. Chem.*, 2010, 4279–4287.
16 Y. Ito, A. Miyazaki, K. Fukui, S. Valiyaveettil, T. Yokoyama and T. Enoki, *J. Phys. Soc. Jpn.*, 2008, **77**, 103701.
17 Y. Ito, A. Miyazaki, S. Valiyaveettil and T. Enoki, *J. Phys. Chem. C*, 2010, **114**, 11699–11702.
18 Y. Ito, K. Takai and T. Enoki, *J. Phys. Chem. C*, 2011, **15**, 8971.
19 K. Okuyama, T. Hasegawa, M. Ito and N. Mikami, *J. Phys. Chem.*, 1984, **88**, 1711–1716.
20 A. V. Abramenkov, A. Almenningen, B. N. Cyvin, S. J. Cyvin, T. Jonvik, L. S. Khaikin, C. Rømming and L. V. Vilkov, *Acta Chem. Scand.*, 1988, **42a**, 674–684.
21 R. Huber, M. T. González, S. Wu, M. Langer, S. Grunder, V. Horhoiu, M. Mayor, M. R. Bryce, C. Wang, R. Jitchati, C. Schönenberger and M. Calame, *J. Am. Chem. Soc.*, 2008, **130**, 1080–1084.

22 A. Mishchenko, D. Vonlanthen, V. Meded, M. Burkle, C. Li, I. V. Pobelov, A. Bagrets, J. K. Viljas, F. Pauly, F. Evers, M. Mayor and T. Wandlowski, *Nano Lett.*, 2010, **10**, 156–163.
23 N. Nakamura, K. Uno and Y. Ogawa, *Acta Crystallogr.*, 2001, **E57**, o505.
24 K. Kuwabara, F. Horii and Y. Ogawa, *J. Mol. Struct.*, 2002, **602**, 79.
25 Y. Ito, A. Miyazaki, K. Takai, V. Sivamurugan, T. Maeno, T. Kadono, M. Kitano, Y. Ogawa, N. Nakamura, M. Hara, S. Valiyaveettil and T. Enoki, *J. Am. Chem. Soc.*, 2011, **133**, 11470–11473.
26 M. J. Frisch, *et al.* Gaussian 09, revision C. 01, Gaussian, Inc., Wallingford CT, 2010.
27 A. D. Becke, *J. Chem. Phys.*, 1993, **98**, 5648.
28 C. Lee, W. Yang and R. G. Parr, *Phys. Rev. B: Condens. Matter Mater. Phys.*, 1988, **37**, 785.
29 M. Head-Gordon, J. A. Pople and M. J. Frisch, *Chem. Phys. Lett.*, 1988, **153**, 503.
30 J. P. Perdew, K. Burke and M. Ernzerhof, *Phys. Rev. Lett.*, 1996, **77**, 3865–3868.
31 J. M. Soler, E. Artacho, J. D. Gale, A. García, J. Junquera, P. Ordejón and D. Sánchez-Portal, *J. Phys.: Condens. Matter*, 2002, **14**, 2745–2779.
32 T. Tada, Y. Yamamoto and S. Watanabe, *Theor. Chem. Acc.*, 2011, **130**, 775–788.
33 The Hamiltonian for only the organic molecular regions in Fig. 1(c) depends on time. From the first-principles MD trajectories, we calculated the dihedral angles θ between neighbouring benzene rings as a function of time. The time-dependent transfer integrals between the corresponding neighbouring benzene rings are obtained as $\tau\cos\theta$, where τ is the transfer integral between neighbouring atoms, and τ = 1.0 eV for adjacent carbons with a distance of 1.4 Å is adopted throughout this study.
34 The expected value of position $<r(t)>$ can be calculated using the wave packet $\phi(t)$ as $<\phi(t)|r(t)|\phi(t)>$.
35 J. G. Kushmerick, D. B. Holt, J. C. Yang, J. Naciri, M. H. Moore and R. Shashidhar, *Phys. Rev. Lett.*, 2002, **89**, 086802.
36 S. U. Jen, *Phys. Rev. B: Condens. Matter Mater. Phys.*, 1992, **45**, 9819–9823.
37 S. U. Jen, T. P. Chen and S. A. Chang, *J. Appl. Phys.*, 1991, **70**, 5831–5833.
38 T. Dadosh, Y. Gordin, R. Krahne, I. Khivrich, D. Mahalu, V. Frydman, J. Sperling, A. Yacoby and I. Bar-Joseph, *Nature*, 2005, **436**, 677–680.
39 P. V. James, P. K. Sudeep, C. H. Suresh and K. G. Thomas, *J. Phys. Chem. A*, 2006, **110**, 4329–4337.
40 J. M. Seminario and P. A. Derosa, *J. Am. Chem. Soc.*, 2001, **123**, 12418–12419.
41 The tunnelling barrier of 0.6τ, corresponding to the transfer integral between the electrode and the single molecule, was adopted in the tight binding model. This barrier parameter leads to a single molecular conductance of $0.01G_0$ for the same linker molecule, which can be recognized as a reasonable value of this single molecular contact for the following reasons: (i) we have no direct experimental data for the conductance of the same linker molecule with Pd electrodes, (ii) the conductance value of the same contact with Pd is calculated to be $\sim 0.1G_0$ in an NEGF-DFT calculation, but this value cannot be adopted as is, because the DFT calculation overestimates the conductance owing to the underestimation of the HOMO–LUMO gap of molecules, (iii) for a similar linker molecule with Au electrodes, the experimental and DFT values are ~ 0.01 and $\sim 0.1G_0$, respectively, and the large difference (*i.e.* one order of magnitude) is caused mainly by the underestimation of the HOMO–LUMO gap in DFT, as mentioned in point (ii), (iv) the electronic states of metals such as Au and Pd are relatively well-described in DFT, and therefore (v) the conductance of the linker molecule with Pd electrodes can be estimated by reducing it one order of magnitude from the DFT value ($0.1G_0$), that is, $0.01G_0$.
42 M. Kiguchi, S. Nakashima, T. Tada, S. Watanabe, S. Tsuda, Y. Tsuji and J. Terao, *Small*, 2012, **8**, 726–730.
43 Y. Selzer, M. A. Cabassi, T. S. Mayer and D. L. Allara, *J. Am. Chem. Soc.*, 2004, **126**, 4052–4053.
44 Y. Selzer, L. Cai, M. A. Cabassi, Y. Yao, J. M. Tour, T. S. Mayer and D. L. Allara, *Nano Lett.*, 2005, **5**, 61–65.
45 We calculated the diffusion coefficients using different trajectories extracted from the MD results for 30 ps and confirmed that the standard deviation (SD) of the calculated mobilities at 50 K is smaller than 0.02 $m^2\ V^{-1}\ s^{-1}$, corresponding to the SD of 6.5 Ω in the calculated resistance.
46 The width parameter W of 30 μm was estimated from the photo images in Fig. 3; thus, the cross section S can be obtained as 30 μm × 5 nm, assuming that the effective region for conduction is realized as the shortest pathway between the electrodes [thin green layer in Fig. 1(b)]. The factor F of 1/10 was simply obtained by taking the volume density of the Pd nanoparticles in the sample into account.

